RICE STRAW ASH: A POTENTIAL POZZOLANIC SUPPLEMENTARY MATERIAL FOR CEMENTING SYSTEMS.

Josefa Roselló [1], Lourdes Soriano [2], M. Pilar Santamarina [3], Jorge L. Akasaki [4], José Monzó [5], Jordi Payá [6,*]

[1] Departamento de Ecosistemas Agroforestales, Universitat Politècnica de València, Spain
e-mail: jrosello@upvnet.upv.es
[2] Instituto de Ciencia y Tecnología del Hormigón ICITECH, Universitat Politècnica de València, Spain
e-mail: lousomar@upvnet.upv.es
[3] Departamento de Ecosistemas Agroforestales, Universitat Politècnica de València, Spain
e-mail: mpsantam@eaf.upv.es
[4] Departamento de Engenharia Civil, Universidade Estadual Paulista Campus Ilha Solteira, Brasil
e-mail: akasaki@dec.feis.unesp.br
[5] Instituto de Ciencia y Tecnología del Hormigón ICITECH, Universitat Politècnica de València, Spain
e-mail: jmmonzo@cst.upv.es
[6] Instituto de Ciencia y Tecnología del Hormigón ICITECH, Universitat Politècnica de València, Spain e-mail: jjpaya@cst.upv.es
*Corresponding autor

List of abbreviations

AWA: agricultural waste ashes
BLA: Bamboo leaf ash
CH: Calcium hydroxide (hydrated lime)
C-S-H: calcium silicate hydrate gel
DTG: Derivative thermogravimetric curves
EDS: energy dispersive x-ray spectroscopy
FESEM: Field emission scanning electron microscopy
FTIR: Fourier transform infrared spectroscopy
OM: optical microscopy
RHA: Rice husk ash
RLA: rice leaf ash
RlsA: rice leaf sheath ash
RsA: rice stem ash
RSA: rice straw ash
SCM: supplementary cementing material
SLA: sugarcane leaf ash
TG: thermogravimetry
XRD: X-ray powder diffraction

Abstract

Biomass waste from rice straw has many management problems, including field firing causing severe air pollution and natural organic decomposition resulting in methane emission. The conversion of this waste to ashes may offer the possibility of reusing them in cementing systems. For the first time ashes from different parts of the rice plant (*Oryza sativa*) were characterized from the chemical composition point of view: rice leaf ash (RLA), rice leaf sheath ash (RlsA) and rice stem ash (RsA). Microscopic studies on ashes revealed heterogeneity in the distribution of chemical elements in the remaining cellular structure (spodograms). The highest concentration of SiO_2 was found in dumbbell-shaped phytoliths (%SiO_2>78%). In the global chemical composition of ashes, SiO_2 was also the main oxide present. According to Vassilev´s classification of chemical composition, RLA belongs to the K-MA zone (medium acid), RlsA to the K-zone (low acid) and RsA to the S-zone (high acid). Calcination temperatures ≥ 550°C completely removed organic matter from the straw and ashes underwent significant sinterisation by calcining at 650ºC due to the presence of potassium chloride. Here, ashes from global straw (rice straw ash, RSA) are characterised (via X-ray diffraction, Fourier transform infrared spectroscopy and thermogravimetry) and tested from a reactivity point of view (reaction towards calcium hydroxide) in order to assess the possibility for its reuse in cementing systems. Results from pastes made by mixing RSA and calcium hydroxide showed that the pozzolanic reactivity of the ashes is important (hydrated lime fixation of 82% for 7 days and 87% for 28 days in RSA:hydrated lime paste) and cementing C-S-H gel is formed after 7 and 28 days at room temperature. Compressive strength development of Portland

cement mortars with 10% and 25% replacements by RSA yielded 107% and 98% of the strength of control mortar after 28 days of curing. Frattini test confirmed the pozzolanicity of the RSA blended cements. These reactivity results are very promising in terms of the potential reuse of ashes in cementing systems.

Keywords: rice straw ash; FESEM; spodogram; chemical composition; amorphous silica; pozzolanic reactivity

1. Introduction

Agricultural wastes are commonly assessed as biomass sources for energy purposes. They can be classified in three groups: energy crops, food production wastes and agricultural wastes (Titiloye et al., 2013). Agricultural wastes are usually composed of straws (leaves and stems) and fruit-shells. Some industrially derived agricultural wastes also include bagasse, cobs, seeds, pods and husks. Huge amounts of these wastes are available and the selection and appropriate treatments of them could provide building and infrastructure materials.

One of the most important challenges related to the production of building materials is focused on their environmental impact (ecological footprint, carbon footprint), mainly on the production of inorganic binders, such as ordinary Portland cement OPC (Barceló et al., 2014). It is well known than the production

of OPC is a very intensive process both in terms of energy and raw materials. About 5% of total worldwide anthropogenic CO_2 emissions are generated from the manufacture of OPC-based cement products (Worrell et al., 2001). Cement production has rapidly increased over the last few decades and reached annual production of 4.3 billion tonnes in 2014 (CEMBUREAU, 2014). Since 1990, the blending compositions of cements have changed significantly (Schneider et al., 2011), which has involved a reduction in clinker content (also named the Clinker factor, CF). The CF value in 2003 was 0.85, whereas in 2010 it was 0.77; the prediction for 2050 is for it to be 0.71 (WBCSD, 2009). This reduction in CF was due to the use of supplementary cementing materials (SCMs). Traditionally (Siddique and Khan, 2011), wastes from industrial activities are blended with Portland cement clinker: ground granulated blast furnace slag, coal fly ash and silica fumes. The first ash from agricultural biomass used in cement or concrete was rice husk ash (RHA) (Mehta, 1983). Utilisation of ashes will contribute to the sustainability of biomass for power generation. Valorisation of bottom ashes, fly ashes and fluidised bed ashes can be carried out by bulk optimisation options: fertiliser and soil amendment, component of building materials or, in the case of carbon-rich ashes, reuse as fuel (Pels and Sarabèr, 2011).

Over the last few decades, greater interest on the development of new SCM derived from agricultural wastes (biomass) is observed in the scientific literature; although the commercialisation of agricultural waste ashes (AWA) and its application in building materials is still scarce (Aprianti et al., 2015). Moreover, in the last years interest has increased regarding the reuse of some biomass-derived ashes in geopolymers (alkali activated materials) to partially

replace the inorganic precursor (Moraes et al., 2016) or totally replace the sodium silicate in the alkaline activator (Bouzón et al., 2014). In both cases, reactive silica in the ashes plays an important role for the development of high-performance geopolymers.

The main basis for the valorisation of these AWA lies in the fact that they contain high amounts of silica. This silica is a basic component required for a pozzolanic reaction. This reaction consists of the acid-base reaction between calcium hydroxide (portlandite, when produced from hydration of Portland cement) and silicon oxide (silica):

$$\mathrm{Ca(OH)_2 + SiO_2 \rightarrow C-S-H\ (gel)}$$

The chemical reaction yields calcium silicate hydrate gel (C-S-H), which has cementing properties. When a SCM presents this behaviour, it is termed a pozzolan and it presents pozzolanic properties. The presence of silica in ash is a necessary factor for a pozzolanic reaction, although it is not the only required factor: a small size of ash particle (high specific surface area) and amorphous state (not crystalline phase) are also required. In some cases, amorphous alumina is also involved in the pozzolanic process.

Over the last few years, interest has increased regarding the study the valorisation of AWA (Vassilev et al., 2013; Pels and Sarabèr, 2011), specifically on the addition of AWA to cements (blended Portland cements, alkali-activated cements) and concrete for the following reasons: (a) biomass is produced

145 worldwide in huge amounts and frequently its management is very complicated;
146 (b) valorisation as livestock food, fertiliser, cellulosic-based derived materials
147 (fibres, boards) are not always available or are not economically viable; (c)
148 energetic valorisation of biomass gained interest as a substitute for fossil fuels
149 since it is technically viable worldwide; (d) the transformation of biomass into
150 AWA is an CO_2 neutral process because the carbon released to the
151 atmosphere during combustion was recently fixed by photosynthesis; (e) the
152 ashes could show pozzolanic properties and be then valorised in building
153 materials and (f) the construction industry has the capacity to take in these
154 ashes due to its large requirements in terms of raw materials.
155
156 Recently, some advances in the application of new AWA in cementing systems
157 were reported, including: ashes from banana leafs (*Musa* sp., Kanning et al.,
158 2014), switchgrass (*Panicum virgatum*) (Wang et al., 2014), elephant grass
159 (*Pennisetum purpureum,* Cordeiro and Sales, 2015), bamboo leaf (*Bambusa*
160 sp., Frías et al., 2012), sugarcane straw (*Saccharum officinarum*, Moraes et al.,
161 2015), barley straw (*Hordeum vulgare*, Cobreros et al., 2015) and plane tree
162 (*Platanus* sp., Binici et al., 2008).
163
164 Rice straw is an agricultural waste that has some management problems: field
165 firing causes severe air pollution and natural organic decomposition favours
166 methane emission (Yuan et al., 2014). This last process has a potent
167 environmental effect in terms of greenhouse gas emission, as the global
168 warming potential of methane is much higher than that of CO_2: 25-times more
169 for a 100 year horizon and 72-times more for 20 year horizon (IPCC, 2007).

Thus, it is crucial to valorise this waste as rice production accounts for 5–10% of worldwide methane emissions. Huge amounts of rice straw are produced worldwide, considering that 1–1.5 kg of straw is generated for every 1 kg of paddy rice (Binod et al., 2010). The worldwide production of rice straw was 731 million tonnes in 2008 (Abdel-Rahman et al., 2015) and Asia was the major producer, generating 620 million tons of the straw (IRRI, 2016). However, scarce research exists on the characterisation of ashes from rice straw ash (RSA) and their potential applications. An interesting approach for obtaining pure silica from rice straw by a sono-assisted sulphuric acid process was reported (Rehman et al., 2013) and Abou-Sekkina et al. (2010) studied three samples of RSA from Egypt and concluded that the silica content was 65% by mass and that no crystalline phases were identified. Ataie et al. (2015) prepared ashes from rice straw and wheat straw after previous treatment with hydrochloric acid and further calcination at 650ºC and 500ºC.

It is well-known that silicon is an element absorbed by the roots of plants in the form of silicic acid, which is transported through the vascular system and deposited in the form of opal or hydrated amorphous silica ($SiO_2.nH_2O$). This silica compound is deposited in: (a) the cellular walls; (b) the interior of the cells (lumen); (c) epidermal appendages (trichomes) and (d) the intercellular spaces in stems and leaves (Prychid et al., 2003). This precipitation process of silica is irreversible (Epstein, 1999): in the three first cases a silica particle replicates the shape of the cellular structure, while for the fourth case no relationship between silica deposit shape and the intercellular space is obtained.

Monocot plants accumulate silica (> 3 mg of Si per g of dried matter), mainly plants belonging to Poaceae family: rice (*Oryza sativa*) and sugarcane (*Saccharum officinarum*) (Ma and Yamaji, 2006). Epidermal tissues in Poaceae species present particular characteristics that are used in taxonomy. Some taxonomic classifications are based on these cellular dispositions: siliceous cells (phytoliths), suberous cells and trichomes. Phytoliths are solid deposits in which silica is the main component. Their size (typically 10–20 microns) and their shape vary significantly depending on the plant. The following main morphotypes are described: dumbbells, saddle and cross; also intermediate shapes can be found (Wilding and Drees, 1971; Piperno, 2006).

In the rice plant, the silica is highly concentrated in the husk (more than 20% by mass of dried husk). Leaves (formed by leaf blades and leaf sheaths) also are silica-rich parts and contain 13% and 12% silica, respectively. Finally, roots store less silica (2%) (Anala and Nambisan, 2015).

The goal of this paper is to characterise different parts of the rice plant (*Oryza sativa*) by means of the identification and analysis of the distribution of chemical elements present in the ash (energy dispersive x-ray spectroscopy, EDS) assessed in terms of the obtained spodogram (optical and field emission scanning electron microscopy), crystalline pattern (X-ray powder diffraction, XRD) and reactivity towards calcium hydroxide (pozzolanic reactivity, reaction products characterisation and hydrated lime fixation) and towards ordinary Portland cement (compressive strength and Frattini test).

2. Materials and methods

Rice straw samples (leaf blade, leaf sheath and stem) were collected in L´Albufera (Valencia, Spain). These samples were stored at 4°C in sealed plastic bags until they were used for the analyses.

Fresh rice straw samples were washed thoroughly to remove residual soil contamination. One squared centimetre sections were prepared by cutting and paradermal lamellae 40 microns thick were prepared using a freezing microtome (Jung AG). These cuts were clarified with a 50% sodium hypochlorite solution and then washed several times with distilled water. Small pieces of rice leaves were heated at 105°C for 24 hours in a laboratory oven (Memmert UN model) for the studies on dried samples. For studies on calcined samples, fresh pieces of leaf blade, leaf sheath and stem were calcined for 1 hour at different selected temperatures (450, 550 and 650°C) in a muffle furnace (Carbolite RHF model 1500). The obtained ashes were: rice leaf ash (RLA), rice leaf sheath ash (RlsA) and rice stem ash (RsA). Furthermore, large samples (20 g) of rice straw were calcined at the same temperatures as above to obtain ashes (RSA), which were used for reactivity studies.

For optical microscopy (OM) studies the cuts of fresh material, once clarified, were stained with safranin-light green, dehydrated and mounted using a synthetic mix of resins (Eukit, Mounting medium for microscope preparation) for observation under a light microscope (Olympus PM-10AK3).

For the field emission scanning electron microscopy (FESEM) selected samples (dried rice leaves and ashes) were studied using a ZEISS ULTRA 55 microscope. Samples were studied at 1 kV and at a working distance of 3–5

mm. Samples for chemical microanalysis (EDS) were not covered and were studied at 15 kV at working distance of 5–7mm.

For reactivity studies, the following equipment was used: Thermogravimetric analysis was performed using a Mettler-Toledo TGA850 instrument. Analysis performed on ashes was carried out in a temperature range of 35–1000ºC at a heating rate of 20ºC.min^{-1} in a dried air atmosphere (75 mL.min^{-1} gas flow) in 70 µL alumina crucibles. Analysis performed on ash:calcium hydroxide pastes was carried out in a temperature range of 35–600ºC at a heating rate of 10ºC.min^{-1} in a nitrogen atmosphere (75 mL.min^{-1} gas flow) in sealed 100 µL pin-holed aluminium crucibles. Fourier transform infrared spectroscopy (FTIR) was performed using a Bruker TENSOR 27 in the wavenumber range between 400 and 4000 cm^{-1}. XRD patterns were obtained by a Bruker AXS D8 Advance with a voltage of 40 kV, current intensity of 20 mA and a Bragg's angle (2θ) in the range of 10–60º.

EDS chemical composition results were submitted to variance analysis (ANOVA) with significant values at $P < 0.05$. Data analysis was performed using Statgraphics Centurion XVI.II.

Mortars were prepared according to UNE-EN 196-1 standard: water/cement ratio was 0.5 and sand/cement ratio was 3. Prismatic specimens (40x40x160 mm) were cast, and after demoulding they were cured under water for 7 and 28 days. Control mortar was prepared by using ordinary Portland cement (OPC), Spanish cement CEM I-52.5R. RSA containing mortars were prepared by replacing 10% and 25% of OPC by RSA. The ash was previously ground and its mean particle diameter was 13 µm. Compressive strength values of mortars

were obtained by means a universal testing machine according to UNE-EN 196-1. Pozzolanicity studies (Frattini test) were carried out according to UNE-EN 196-5.

3. Results and discussion

The rice straw is a mixture of different parts of the rice plant and usually contains leaf blades, leaf sheaths and stems. The easiest part to study using microscopy is the leaf blade, as it is thinner (from hereon in, we refer to leaf blade as ‘leaf’). When calcining leaf, the spodogram is maintained and different parts of the cells and structures can be identified. This is why the first analyses were conducted on the rice leaf and the ashes obtained after the various temperature treatments. Ashes obtained from leaf sheaths and stems will be discussed later in the manuscript. Finally, an approach to reactivity studies from the pozzolanic point of view will be discussed using ash produced from a mixture of the different parts in the straw.

3.1 Microscopic studies on fresh leaves

Optical microscopy studies on fresh rice leaves were carried out in order to understand the character of cells in the tissue. The upper (adaxial) and the lower leaf surfaces (abaxial) were analysed. In the adaxial surface image (Fig.1a) trichomes and phytoliths were easily identified. The phytolits showed a bilobated shape and the major axis of the phytoliths was perpendicular (Fig.1b) to the longitudinal axis of the leaf (bambusoide dermotype (Prat, 1936)). Phytoliths are arranged short distances from each other and among them

294 suberous cells are disposed. Elongated epidermal cells and stomata are
295 displayed surrounding the aligned phytoliths and suberous cells.

296

297 INSERT Fig. 1.

298

299 *3.2 Microscopic studies on dried leaves*

300 Some leaves were dried at 105°C for FESEM studies (Fig. 2). In these
301 conditions, free water was released and organic and inorganic structures were
302 maintained in their original arrangements. Both surfaces (Fig. 2a and 2b:
303 adaxial; Fig. 2c and 2d, abaxial) presented the same type of epidermal cells and
304 structures. After the drying process, the shape of phytoliths was revealed: some
305 of them seemed to be dumbbell shape (Fig. 2b and 2d). Apparently, the shape
306 of phytoliths is not homogeneous within the leaf (some appear as a cross
307 shape). Stomata appeared aligned in parallel to the phytoliths arrangement.
308 Abaxial surface showed a wavier form.

309

310 INSERT Fig. 2.

311

312 *3.3 Microscopies studies on calcined leaves*

313 Calcination of leaves was carried out to remove organic components. Thus, the
314 spodogram (structural residue resulting from the removal of organic matter by
315 burning, which maintains the leaf's structure) was clearly observed. Samples of

316 leaves were calcined at different temperatures, 450, 550, 600 and 650°C, for 1
317 hour. Then, they were studied by FESEM. Samples obtained at 450, 550 and
318 650°C were also assessed by EDS.

319

320 Figure 3 shows some micrographs corresponding to samples calcined at 450°C.
321 It can be noted than some parts of the leaf maintained a similar structure to the
322 dried samples: the spodogram at 450°C maintained the original arrangement.
323 Thus, aligned phytoliths are surrounded with an inorganic matrix (Fig. 3a and
324 3b) and stomata are arranged parallel to phytoliths (Fig. 3a). However, the
325 original structure is not maintained for other parts of the leaf, as can be seen in
326 Figure 3c. Only phytolith chains were unaltered. In Figure 3d, a detailed view of
327 some phytoliths is shown, in which their dumbbell shape is highlighted. The
328 removal of organic matter rendered the real shape for the phytoliths. Some EDS
329 analysis (spots) were carried out in order to compare the chemical composition
330 of the ashes. Table 1 summarises the chemical composition (in oxide form, by
331 mass) for four selected spots (two phytoliths and two matrix spots). It is very
332 noticeable that phytoliths are mainly formed of SiO_2 and K_2O (more than 90%)
333 and the surrounding matrix presents more elements in significant percentages:
334 Cl, P_2O_5, SO_3, CaO and MgO. SiO_2 in the matrix was less than half that value
335 found in phytoliths, while K_2O increased by twofold. These results reflect the
336 heterogeneity in the disposition of inorganic elements in the ash. Thus,
337 recording 15 EDS signals from 10000 μm^2 areas, on both abaxial and adaxial
338 surfaces, carried out a general analysis. The mean composition results are
339 summarised in Table 2. Chemical compositions of each area analysed were
340 different and this behaviour is reflected in the standard deviation values for

oxide contents. The mean values for the main oxides were: 38.0% and 43.4% SiO_2 for adaxial and abaxial surfaces and 28.1% and 27.0% for K_2O. From the statistical analysis (comparison of mean values from two populations, that is adaxial and abaxial surfaces), it can be concluded that all compound contents are not significantly different, except for chloride and Na_2O ($P < 0.05$).

INSERT TABLE 1

INSERT TABLE 2

INSERT Fig. 3.

The chemical composition of the RLA was similar to that found for sugarcane leaf ash (SLA) calcined at the same temperature (Roselló et al., 2015). In this case, the SiO_2 content was higher (mean value of 40.7% for RLA versus 30.0% for SLA); K_2O content was similar (27.5% vs 29.0%, respectively). The most important difference is in the chloride content, which was much lower for RLA than in SLA (1.0% vs 4.0%, respectively). This fact becomes crucial for applications in cements and concrete (Angst et al., 2009) because the presence of chloride ions favours the corrosion of steel in reinforced concrete; thus, RLA will be better in terms of corrosion behaviour. Regarding other elements, RLA presented lower contents of alkaline earth oxides (CaO and MgO) and higher in P_2O_5. The SO_3 contents were similar for both RLA and SLA.

Vassilev et al (2010) proposed a classification of biomass ashes according to the chemical composition (Fig. 4). Thus, they designed a ternary diagram in which the corners were occupied by the sum of selected oxide contents: (a) the sum of silicon, aluminium, iron, sodium and titanium oxides (this will be referred

365 to as σ in this manuscript); (b) the sum of calcium, magnesium and manganese
366 oxides (τ) and (c) the sum of potassium, phosphorus, sulphur and chlorine
367 oxides (κ). In this way, seven zones were defined, depending on the proportion
368 of these groups of oxides in the ash. Rice husk ash (RHA) is a typically
369 siliceous ash, with very low content of other oxides and consequently is
370 represented in the S-type ash zone. Bamboo leaf ash (BLA) is also located in
371 the S-type zone, as it has similar composition, although it is richer in potassium.
372 Biomass ashes from herbaceous and agricultural grass, straw and residues are
373 located in K-type and K-MA-type zones. This is the case of RLA, which is
374 located in K-MA zone: σ = 51.2%, τ = 11.1%, κ = 47.7%. Very close but in K-
375 type zone, is located SLA (from Roselló et al., 2015: σ = 30.3%, τ = 24.4%, κ =
376 45.4%).

377

378 INSERT Fig. 4.

379

380 In Figure 5 the spodogram of the adaxial surface for RLA obtained at 550°C is
381 observed. Some line-arranged dumbbell phytoliths were identified (Fig. 5a)
382 surrounded by a smooth inorganic matrix. Interestingly, when the images are
383 magnified (Figs. 5b, 5c and 5d), one can see that the phytholiths have rounded
384 edges (compare to Fig. 3d) and some of them are connected along certain
385 sides. Apparently, this deformation is related to a semi-fusion or sinterisation
386 process carried out during the calcination.

387 The same behaviour was observed for the abaxial surface (Fig. 6). In Figure 6a
388 and 6b a double chain of phytoliths corresponding to the longitudinal centre of

389 the leaf (midrib, the central vein of the leaf) is shown. Figure 6c shows highly
390 altered phytoliths, probably due to a focalised high temperature during
391 calcination. In Figure 6d, a picture of the inorganic matrix after organic matter
392 removal is shown: in this case, more rounded structures are observed
393 compared to the matrix depicted in Figure 3d.

394

395 INSERT Fig. 5.

396

397 INSERT Fig. 6.

398

399 The melting point of ashes depends on the percentage of inorganic elements
400 (Biedermann, et al., 2015). Thus, high percentages of alkalis (Na, K) and
401 chlorides result in a decrease in melting temperatures; on the contrary,
402 presence of alkaline earth elements (Ca, Mg) increasing it. In general, straw
403 ashes with low Ca content and high K and Si contents start to sinter and melt at
404 lower temperatures than wood ashes (which are richer in Ca) (Biedermann, et
405 al., 2015). Potassium is the key element that participates in the formation of
406 troublesome species (e.g., formation of potassium salts, such as KCl and
407 K_2SO_4). The K_2O-SiO_2 binary system starts to melt in the range of 600–700°C
408 (Wang et al., 2012). Despite the temperature furnace being 550ºC,
409 temperatures on the surface of the materials were probably higher as the
410 combustion of organic matter released a significant quantity of heat. In these
411 conditions, the temperature close to the sample was certainly higher than
412 600°C. This is the reason why all remaining structures after burning at 550°C

appeared rounded. Furthermore, the matrix surrounding the phytoliths was affected: in this case, the presence of Ca and Mg did not prevent the sintering/melting process, as can be seen in Figure 6d for the matrix in the abaxial surface of rice leaf burned at 550°C. This behaviour supports the relationship between initial deformation temperature (IDT) and the K_2O content observed for biomass ashes, whereby IDT lowered when K_2O increased (Niu et al., 2010).

INSERT Fig. 7.

The chemical composition of RLA calcined at 550°C was also determined by EDS (eight individual analyses were carried out). Mean values are given in Table 2. In this case, statistical analysis shown that there are differences ($P < 0.05$) in Cl, CaO, MgO and SO_3 contents when compared with sample prepared at 450°C.

RLA samples also were obtained by calcining the straw at 600 and 650°C. Figure 7 shows selected FESEM micrographs. Phytoliths in Figure 7a, 7b and 7c showed that spodograms of ashes calcined at 600°C appeared slightly sintered. In samples obtained at 650°C, the sinterisation effect is highlighted: many phytoliths changed from their original shape to rounded dumbbell shape (Fig. 7d), spheroidal structures (Fig. 7e) or to produce a continuous line through the merging of phytoliths (Fig. 7f).

EDS analyses were performed on samples obtained at 650°C. The calculated chemical compositions did not vary significantly with respect to those obtained

437 at lower temperatures, except for chloride content. These analyses yield
438 chloride contents in the range 0.15–0.04%. This means that there was a
439 removal of chlorides during treatment at this temperature. Probably, the chlorine
440 was removed in the form of potassium chloride by volatilisation due to the low
441 melting point of this salt (776°C).

442

443 *3.4 Microscopic studies on rice leaf sheath and rice stem ashes*

444 Samples of leaf sheath (ls) and stem (s) were calcined at 450°C. FESEM
445 micrographs of the obtained ashes (RlsA and RsA, respectively) are showed in
446 Figure 8. External parts (Figs. 8a and 8c) showed phytoliths and similar texture
447 to that of leaf blades described above. However, internal structures (Figs. 8b
448 and 8d) were different and a very porous skeleton was identified. Chemical
449 analysis (EDS) of the ashes was conducted in order to compare the
450 percentages of the main oxides. Values are summarised in Table 3. Statistical
451 analysis showed that the chemical compositions for RLA and RlsA are different
452 ($P < 0.05$) for all oxides, except for SiO_2. The SiO_2 content was higher for the
453 external part of the leaf sheath (37.7%) than for the internal part (23.3%),
454 although the difference is not statistically significant. Significant differences ($P <$
455 0.05) were only found for K_2O, SO_3 and Na_2O. Interestingly, K_2O and chloride
456 contents were higher for RlsA than RLA: chloride content was more than five
457 times greater in RlsA. In the Vassilev´s ternary diagram (see Fig. 4), RlsA
458 belongs to K-zone (σ = 32.6%, τ = 4.2%, κ = 63.2%).

459 On the contrary RsA showed a high percentage of SiO_2 (mean value 84.3%).
460 Obviously, the rest of components were low, especially chloride, which scarcely

461 reached 0.1%. From a statistical point of view, there is a significant difference
462 ($P < 0.05$) between all oxides, except CaO and Na_2O, with respect to the RLA.
463 Thus, the position of RLA in the Vassilev´s diagram (See Fig 4a) is in the S-
464 zone: σ = 84.7%, τ = 8.7%, κ = 6.6%.

465

466 INSERT TABLE 3

467 INSERT Fig. 8.

468

469

470 *3.5 Reactivity studies on rice straw ashes*

471 In general terms, rice straw collected from the field is composed of leafs, stems
472 and leaf sheaths; additionally, is very common that some soil particles (sand,
473 clays, feldspar) appear together the biomass. In this study, a sample of rice
474 straw was collected and calcined in order to analyse the pozzolanic properties
475 of the ash. Three calcining temperatures (450°C, 550°C and 650°C) were
476 selected for producing the corresponding ashes (RSA-450, RSA-550, RSA-
477 650).

478 These samples were characterised by means of thermogravimetry (TG), FTIR
479 and powder XRD.

480 The thermogravimetric analysis curve (Fig. 9) for RSA-450 showed that
481 decomposition of the organic matter/carbon was not completed at 450°C,
482 although there was a mass loss (6.92%) in the 350–650°C range. Also a mass
483 loss was beginning at 900°C, which is related to the fusion/evaporation of

potassium sulphate (pure K_2SO_4 melts at 1069°C). Conversely, the sample obtained at 550°C did not show (Fig. 9) any significant mass loss related to organic matter/carbon, which means that this temperature is enough for removing organic compounds in rice straw; RSA-550°C also shows a similar initiation of mass loss at 900°C.

FTIR spectra for these ashes are depicted in Figure 10. The main absorption bands are related to Si-O vibrations, in accordance with the siliceous nature of the ashes. The most intense bands are 1056 – 1035, 795 – 785, 617 and 453 cm^{-1}. Also, absorption bands related to the presence of carbonate anions (probably due to the presence of calcium carbonate) are observed: 1411–1406 and 877 cm^{-1}. These C-O bands disappeared for RSA-650, suggesting that the small amount of carbonate present in the ash is decomposed (decarbonation) at 650°C.

INSERT Fig. 9.

INSERT Fig. 10.

Finally, in order to complete the characterisation of the ashes, XRD patterns were collected (Fig. 11). Significant major peaks (28.4º and 40.6º) are related to the presence of sylvite (KCl, PDFcard 411476). This crystalline compound is easily identified because solid phases in ashes are mainly amorphous in nature. The baseline deviation in the range 2θ = 15–30° is representative of amorphous

507 silica. Some traces of quartz (SiO_2, PDFcard 331161) are probably due to soil
508 contamination of the rice straw. Interestingly, there was no evidence of the
509 formation of cristobalite or trydimite. This means that conversion of the straw
510 into ashes at a temperature in the 450–650ºC range, does not achieve the
511 crystallisation of amorphous silica. This behaviour has an important
512 consequence because the pozzolanic reactivity of ashes depends on the silica
513 phases: crystalline phases do not react easily towards calcium hydroxide (CH),
514 whereas amorphous silica reacts at room temperature in wet conditions.
515 Secondary minerals are also present in the ashes: arcanite (K_2SO_4, PDFcard
516 050613) and calcite ($CaCO_3$, PDFcard 050586). The peaks corresponding to
517 calcite have less intensity in the RSA-650 sample, confirming the decomposition
518 of the carbonated mineral at this temperature, as suggested from FTIR results.

519

520 INSERT Fig. 11.

521

522 In order to quantify the reactivity of RSA samples, selected mixtures with
523 calcium hydroxide ($Ca(OH)_2$, CH) were prepared and hydrated. Pastes with
524 RSA-450 and RSA-550, prepared with a RSA:CH (1:1) mass ratio were
525 characterised by thermogravimetry (after 7 and 28 days hydration). Derivative
526 thermogravimetric curves (DTG) of RSA-450 pastes are depicted in Fig. 12. In
527 both DTG curves (7 and 28 days), a peak centred at about 150°C was present,
528 related to the dehydration process of calcium silicate hydrate (C-S-H). This
529 compound is typically produced as consequence of the pozzolanic reaction
530 between amorphous silica and CH. Also, a peak appeared at 450°C related to

531 the decomposition of the small amount of remaining ($Ca(OH)_2$). The total mass
532 loss for the temperature range of 35–600°C was very high: 16.09% for 7 days
533 and 15.47% for 28 days; conversely, the mass loss attributed to CH was very
534 low (2.15 and 1.63%, respectively). These data revealed that the pozzolanic
535 reaction was fast and that most of the reaction products were produced in the
536 first 7 days of hydration. This behaviour implies the amorphous nature of the
537 silica present in the ash. The total amount of CH fixed by the RSA-450 ash was
538 very high: 82% for 7 days and 87% for 28 days. Similar results were found for
539 RSA-550, suggesting that both calcining temperatures yielded excellent reactive
540 ashes.

541

542 INSERT Fig. 12.

543

544 RSA-650 reactivity was also assessed by means of the reactivity towards
545 calcium hydroxide in a RSA:CH (3:7) ratio. In this case, with respect to the
546 above-mentioned pastes, the relative amount of CH is much higher (70%). In
547 these conditions, this reagent was in high excess and will be not totally
548 consumed, as can be seen in the TG curves for 7 and 28 days of curing
549 depicted Figure 13. In these curves, a mass loss in the range 540–580°C
550 corresponding to the decomposition of $Ca(OH)_2$ was observed. From the
551 corresponding calculated mass losses for both curing ages, it can be stated that
552 40% and 54%, respectively, of the $Ca(OH)_2$ was chemically combined in the
553 reaction. In the TG curve, mass loss related to the dehydration of C-S-H gel
554 (range 120–200°C) is also observed, similar to that found in 1:1 pastes.

555

556

557 INSERT Fig. 13.

558

559 These pastes also were characterised by means XRD. In Figure 14, XRD
560 patterns for 1:1 RSA-450:CH paste and 3:7 RSA-650:CH paste, both cured at
561 room temperature for 28 days, are shown. Firstly, for the paste with the lowest
562 CH proportion (1:1 paste), it may be noticed that the baseline deviation, which
563 occurred in the ash (see Fig. 11), practically disappeared and the baseline
564 deviation moved to a higher diffraction angle range (2θ = 27–33°). This was due
565 to the transformation of the amorphous silica to C-S-H gel as a consequence of
566 the pozzolanic reaction. The most intense and broad peak was found at 2θ =
567 29.9°, which corresponds to the tobermoritic phase ($Ca_5Si_6O_{16}(OH)_2 \bullet 4(H_2O)$)
568 and this peak overlapped the main peak of calcite (which was present in the ash
569 and also as an impurity in the calcium hydroxide used as reagent for the paste
570 preparation). Furthermore, peaks belonging to sylvite and arcanite were easily
571 identified. Additionally, main peaks from the portlandite ($Ca(OH)_2$,
572 PDFcard040733) also are shown: these peaks were of low intensity,
573 demonstrating the low remaining quantity of portlandite in the paste after 28
574 days of curing. These results corroborate those from the thermogravimetric
575 studies and confirm the high reactivity of the ash towards CH in the pozzolanic
576 process. For the paste with the highest CH proportion (3:7 paste) and because
577 important part of the calcium hydroxide remained unreacted after 28 days of
578 curing (assessed by thermogravimetric analysis), the most intense peaks

observed (Fig. 14) belonging to portlandite. Also, calcite was identified as the main crystalline component because of its presence in the CH reagent. Sylvite and arcanite were not observed due to the intensity of the portlandite peaks. For the same reason the tobermoritic phase was also difficult to observe.

INSERT Fig. 14.

Reactivity of RSA was also assessed by means compressive strength of mortars and pozzolanicity test (Fratini). Blended cements by mixing OPC and RSA were prepared: 10% and 25% replacement percentages of RSA were tested. Results from the Frattini test obtained after 8 days of reaction at 40ºC are showed in Fig. 15. It can be noticed that the points corresponding to RSA containing blends are below the saturation curve. This behaviour confirms the pozzolanic reactivity of the ash.

Mortars cured after 7 and 28 days of curing were tested in compression (six values for each cement and for each curing time). Compressive strengths are summarized in Table 4. Mortar with 10% RSA reached 98.4% of the strength found for OPC control after 7 days, and 107.1% after 28 days; and mortar with 25% RSA reached 83.3% at 7 days and 98.4% after 28 days. All these results confirmed the high pozzolanic reactivity of RSA and the strong contribution of this type of reactivity on the strength development of mortars.

INSERT Fig. 15

602 INSERT Table 4.

603

604 **4. Conclusions**

605 RSA is characterised from microscopic, chemical composition and reactivity
606 point of views. Different parts of the rice straw have different chemical
607 compositions when transformed to ashes: rice leaf ash (RLA), rice leaf sheath
608 ash (RlsA) and rice stem ash (RsA).

609 Microscopic studies (optical and FESEM) revealed heterogeneity in the
610 distribution of chemical elements in ashes according to the cellular structure
611 remaining after organic matter removal (spodograms). The highest
612 concentration of SiO_2 was found for dumbbell shape phytoliths. In the global
613 chemical composition of ashes, SiO_2 was the main oxide present and K_2O was
614 the second main oxide for RLA and RlsA, whereas CaO was the second most
615 abundant for RsA.

616 RLA presented a mean chemical composition with 40.7% SiO_2 and 27.5% K_2O.
617 Also chloride content was relatively high (1.0% by mass). According to
618 Vassilev´s classification, this ash belongs to the K-MA zone (medium acid).
619 These ashes suffer significant sinterisation at 650°C due to the presence of
620 potassium chloride. RlsA was classified accordingly to Vassilev`s in the K-zone
621 (low acid) because of its low SiO_2 content and high K_2O percentage. Noticeably,
622 chloride content found for this ash was five-times greater than that found for
623 RLA. RsA presented a very high SiO_2 percentage (84.3%) and it was classified
624 in the S-zone (high acid).

RSA was tested from the reactivity point of view in order to assess the possibilities for its reuse in cementing systems. Results from pastes made by mixing RSA and calcium hydroxide showed that the pozzolanic reactivity of the ashes is important and cementing C-S-H gel is formed after 7 and 28 days at room temperature. This reactivity was due to the amorphous nature of the silica (SiO_2) in the ash. RSA:CH (1:1) pastes showed a fixation of 85% of available calcium hydroxide and (3:7) pastes a fixation of 54%. OPC-RSA blended cements showed a good performance in terms of compressive strength development, and 107% and 98% of the strength for the control mortar was achieved after 28 of curing for 10% and 25% RSA replacement percentages.

These reactivity results are very promising for the reuse of ashes from this biomass (rice straw) in cementing systems, e.g., as pozzolanic supplementary materials in Portland cement or also as silica-based supplementary precursor for geopolymers (alkali activated materials).

Acknowledgements

The authors acknowledge the financial support of the Ministerio de Economía y Competitividad MINECO, Spain, and FEDER funding [Project: BIA2015-70107-R]. The authors thank the Electron Microscopy Service of the Universitat Politècnica de València (Spain).

References

Abdel-Rahman, M.A., Abdel-Shakour, E.H., Hassan, S.E., Refaat, B.M., Nour El-Din, M., Ewais, E.E., Alrefaey, H.M.A., 2015. Effects on environmental factors and compost additives on *Bacillus sonorensis* 7-1v, a cellulytic strain able to degrade rice straw under solid state fermentation. Int. J. Adv. Res. Biol. Sci 2, 241-251.

Abou-Sekkina, M.M., Issa, R.M., A. Bastawisy, A.E.M., El-Helece, W.A., 2010. Characterization and evaluation of thermodynamic parameters for Egyptian heap fired Rice Straw Ash (RSA). Int. J. Chem. 2, 81-88.

Anala, R., Nambisan, P., 2015. Study of morphology and chemical composition of phytoliths on the surface of paddy straw. Paddy Water Environ. 13, 521-527. http://dx.doi.org/10.1007/s10333-014-0468-5.

Angst, U., Elsener, B., Larsen, C.L., Vennesland, O., 2009. Critical chloride content in reinforced concrete — A review. Cem. Concr. Res. 39, 1122-1138. http://dx.doi.org/10.1016/j.cemconres.2009.08.006

Aprianti, E., Shafigh, P., Bahri, S., Farahani, J.N., 2015. Supplementary cementitious materials origin from agricultural wastes – A Review. Constr. Build. Mater. 74,176-187. http://dx.doi.org/10.1016/j.conbuildmat.2014.10.010

Ataie, F.F., Juenger M.C.G., Taylor-Lange S.C., Riding K.A., 2015. Comparison of the retarding mechanisms of zinc oxide and sucrose on cement hydration and

673 interactions with supplementary cementitious materials. Cem. Concr. Res. 72,
674 128-136.
675 http:// dx.doi.org/10.1016/j.cemconres.2015.02.023
676
677 Barceló, L., Kline, J., Walenta, G., Gartner, E., 2014. Cement and carbon
678 emissions. Mater. Struct. 47 (6), 1055-1065.
679 http://dx.doi.org/10.1617/s11527-013-0114-5
680
681 Biedermann, F., Obernberger, F., 2015. Ash-related problems during biomass
682 combustion and possibilities for a sustainable ash utilization.
683 http://www.bios-bioenergy.at/uploads/media/Paper-Biedermann-AshRelated-
684 2005-10-11.pdf (accessed 28.07.16).
685
686 Binici, H., Yucegok, F., Aksogan, O., KaplaN, H., 2008. Effect of corncob, wheat
687 straw, and plane leaf ashes as mineral admixtures on concrete durability. J.
688 Mater. Civ. Eng. 20, 478-483.
689 http://dx.doi.org/10.1061/(ASCE)0899-1561(2008)20:7(478)
690
691 Binod, P., Sindhu, R., Singhania, R.R., Vikram, S., Devi, L., Nagalakshmi, S.,
692 Kurien, N., Sukumaran, R.K., Pandey, A., 2010. Bioethanol production from rice
693 straw: An overview. Bioresour. Technol. 101, 4767-4774.
694 http://dx.doi.org/10.1016/j.biortech.2009.10.079
695

696 Bouzón N., Payá J., Borrachero M.V., Soriano L., Tashima M.M., Monzó J., 2014.
697 Refluxed rice husk ash/NaOH suspension for preparing alkali activated binders.
698 Mater. Lett. 115, 72-74.
699 http://dx.doi.org/10.1016/j.matlet.2013.10.001
700
701 CEMBUREAU. Activity Report, 2014.
702 http://www.cembureau.eu/sites/default/files/Activity%20Report%202014_websit
703 e_1.pdf (accessed 28.07.16).
704
705 Cobreros, C., Reyes-Araiza, J.L., Nava, R., Rodríguez, M., Mondragón-Figueroa,
706 M., Apatiga, L.M., Rivera-Muñoz, E.M., 2015. Barley straw ash: pozzolanic
707 activity and comparison with other natural and artificial pozzolans from Mexico.
708 Bioresources 10, 3757-3774.
709 http://dx.doi.org/10.15376/biores.10.2.3757-3774
710
711 Cordeiro, G.C., Sales, C.P., 2015. Pozzolanic activity of elephant grass ash and
712 its influence on the mechanical properties of concrete. Cem. Concr. Compos. 55,
713 331–336.
714 http://dx.doi.org/10.1016/j.cemconcomp.2014.09.019
715
716 Epstein, E., 1999. Silicon. Annu. Rev. Plant Physiol. Plant Mol. Biol. 50, 641-664.
717 http://dx.doi.org/10.1146/annurev.arplant.50.1.641
718

719 Frías, M., Savastano, H., Villar, E., Sánchez de Rojas, M.I., Santos, S., 2012.
720 Characterization and properties of blended cement matrices containing activated
721 bamboo leaf wastes. Cem. Concr. Compos. 34, 1019-1023.
722 http://dx.doi.org/ 10.1016/j.cemconcomp.2012.05.005
723
724 IPCC International Panel on Climate Change. Climate Change, 2007 The
725 Physical Science Basis. Cambridge University Press, Cambridge.
726 https://www.ipcc.ch/publications_and_data/publications_ipcc_fourth_assessme
727 nt_report_wg1_report_the_physical_science_basis.htm (accessed 28.07.16).
728
729 IRRI International Rice Research Institute
730 http://irri.org/our-work/research/value-added-rice/rice-straw-and-husks/
731 (accessed 28.07.16).
732
733 Kanning, R.C., Portella, K.F., Bragança, M.O.G.P., Bonato, M.M., Jeannette
734 C.M., Dos Santos, J.C.M., 2014. Banana leaves ashes as pozzolan for concrete
735 and mortar of Portland cement. Constr. Build. Mater. 54, 460-465.
736 http://dx.doi.org/10.1016/j.conbuildmat.2013.12.030
737
738 Ma J.F., Yamaji, N., 2006. Silicon uptake and accumulation in higher plants.
739 Trends Plant Sci. 11, 392-397.
740 http://dx.doi.org/10.1016/j.tplants.2006.06.007
741

742 Mehta, P.K., 1983. Pozzolanic and Cementitious Byproducts as Mineral
743 Admixtures for Concrete - A Critical Review. ACI Special Publication 79 (46
744 pages). American Concrete Institute.
745
746 Moraes, J.C.B., Akasaki, J.L., Melges, J.L.P., Monzó, J., Borrachero, M.V.,
747 Soriano, L., Payá, J., Tashima, M.M., 2015. Assessment of sugar cane straw ash
748 (SCSA) as pozzolanic material in blended Portland cement: Microstructural
749 characterization of pastes and mechanical strength of mortars. Constr. Build.
750 Mater. 94, 670-677.
751 http://dx.doi.org/10.1016/j.conbuildmat.2015.07.108
752
753 Moraes J.C.B., Tashima M.M., Akasaki J.L., Melges J.L.P., Monzó J., Borrachero
754 M.V., Soriano L., Payá J., 2016. Increasing the sustainability of alkali-activated
755 binders: the use of sugar cane straw ash (SCSA). Constr. Build. Mater. 124,148–
756 154.
757 http://dx.doi.org/10.1016/j.conbuildmat.2016.07.090
758
759 Niu, Y., Tan, H., Wang, X., Liu, Z., Liu, H., Liu, Y., Xu, T., 2010. Study on fusion
760 characteristics of biomass ash. Bioresour. Technol.101, 9373-9381.
761 http://dx.doi.org/10.1016/j.biortech.2010.06.144
762
763 Pels, J.R., Sarabèr, A.J., 2011. Utilization of Biomass Ashes, in: Grammelis, P.
764 (Ed.), Solid Biofuels for Energy (series Green Energy and Technology). Springer-
765 Verlag London pp. 219-235.
766 http://dx.doi.org/10.1007/978-1-84996-393-0_10

Piperno, D.R., 2006. Phytoliths: A comprehensive guide for archaeologists and paleoecologists. AltaMira Press, Oxford.

Prat, H., 1936. La Systematique des Graminées: Annals des Sciences Naturelles. Series 10, Botanique, Paris.

Prychid, C.J., Rudall, P.J., Gregory, M., 2003. Systematics and biology of silica bodies in monocotyledons. Bot. Rev. 69, 377-440. http://dx.doi.org/10.1663/0006-8101(2004)069[0377:SABOSB]2.0.CO;2

Rehman, M.S.U., Umer, M.A., Rashid, N., Kima, I., Han, J., 2013. Sono-assisted sulfuric acid process for economical recovery of fermentable sugars and mesoporous pure silica from rice straw. Ind. Crops Prod. 49, 705-711. http://dx.doi.org/10.1016/j.indcrop.2013.06.034

Roselló, J., Soriano, L., Santamarina, M.P., Akasaki, J.L., Melges, J.L.P., Payá, J., 2015. Microscopy Characterization of Silica-Rich Agrowastes to be used in Cement Binders: Bamboo and Sugarcane Leaves. Microsc. Microanal. 21, 1314–1326. http://dx.doi.org/10.1017/S1431927615015019

Schneider, M., Romer, M., Tschudin, M., Bolio, H., 2011. Sustainable cement production-present and future. Cem. Concr. Res. 41, 642-650. http://dx.doi.org/10.1016/j.cemconres.2011.03.019

792 Siddique, R., Khan, M.I., 2011. Supplementary cementing materials, Springer-
793 Verlag Berlin Heidelberg.
794 http://dx.doi.org/10.1007/978-3-642-17866-5
795
796 Titiloye, J.O., Bakar, M.S.A., Odetoye, T.E., 2013. Thermochemical
797 characterisation of agricultural wastes from West Africa. Ind. Crops Prod. 47, 199-
798 203.
799 http://dx.doi.org/10.1016/j.indcrop.2013.03.011
800
801 Vassilev, S.V., Baxter, D., Andersen, L.K., Vassileva, C.G., 2010. An overview of
802 the chemical composition of biomass. Fuel 89, 913-933.
803 http://dx.doi.org/10.1016/j.fuel.2009.10.022
804
805 Vassilev, S.V., Baxter, D., Andersen, L.K., Vassileva, C.G., 2013. An overview of
806 the composition and application of biomass ash. Part 2. Potential utilisation,
807 technological and ecological advantages and challenges. Fuel 105, 19-39.
808 http://dx.doi.org/ 10.1016/j.fuel.2012.10.001
809
810 Wang, L., Hustad, J.E., Skreiberg, Ø., Skjevrak, G., Grønli, M., 2012. A critical
811 review on additives to reduce ash related operation problems in biomass
812 combustion applications. Energy Procedia 20, 20-29.
813 http://dx.doi.org/ 10.1016/j.egypro.2012.03.004
814

Wang, Y., Shao, Y., Matovic, M.D., Whalen, J. K., 2014. Recycling of switchgrass combustion ash in cement: Characteristics and pozzolanic activity with chemical accelerators. Constr. Build. Mater. 73, 472-478. http://dx.doi.org/ 10.1016/j.conbuildmat.2014.09.114

WBCSD. Cement Technology Roadmap 2009 World Business Council for Sustainable Development, Geneva, Switzerland. https://www.iea.org/media/freepublications/technologyroadmaps/cementroadmapreferences.pdf (accessed 28.07.16).

Wilding, L.P., Drees, L.R., 1971. Biogenic opal in Ohio soils. Soil Sci. Soc. Am. Proc. 35, 1004-1010. http://dx.doi.org/10.2136/sssaj1971.03615995003500060041x

Worrell, E., Price, L., Martin, N., Hendriks, C., Ozawa Meida, L., 2001. Carbon dioxide emissions from the global cement industry. Annu. Rev. Energ. Environ. 26, 303-329. http://dx.doi.org/ 10.1146/annurev.energy.26.1.303

Yuan, Q., Pump, J., Conrad, R., 2014. Straw application in paddy soil enhances methane production also from other carbon sources. Biogeosci. 11, 237-246. http://dx.doi.org/10.5194/bg-11-237-2014

841 Table 1. Spot chemical compositions (EDS, % by mass) for rice leaf ash obtained at 450°C (spots
842 identified in Fig. 3).
843

Spot analysis	SiO_2	K_2O	Cl	CaO	MgO	P_2O_5	SO_3	Na_2O
phytolith 1 (Fig 3a)	86.2	8.4	1.0	0.1	0.8	1.6	0.7	1.3
matrix 1 (Fig 3a)	40.0	23.8	6.7	4.0	4.6	12.8	6.0	2.2
phytolit 2 (Fig 3b)	78.2	11.8	1.9	1.2	1.2	1.7	2.0	2.0
matrix 2 (Fig 3b)	25.8	27.4	5.8	11.3	6.7	10.3	10.8	2.0

844
845

Table 2. Mean values of chemical composition for RLA (adaxial, abaxial and both zones) obtained at 450°C and 550°C. Values were calculated from EDS analysis on 115 μm × 85 μm area. (Std. Dev = standard deviation; Max = maximum recorded value; Min = minimum recorded value)

Sample	Parameter	SiO_2	K_2O	Cl	CaO	MgO	P_2O_5	SO_3	Na_2O
RLA 450ºC adaxial (1)	Mean value	38.0	28.1	1.2	6.2	5.9	13.6	6.5	0.6
	Std. Dev.	13.4	5.6	0.3	2.0	2.1	5.2	1.6	0.2
	Max.	62.5	37.2	1.6	9.0	10.7	24.2	9.3	1.2
	Min.	15.5	20.0	0.9	3.0	2.7	6.1	4.0	0.3
RLA 450ºC abaxial (2)	Mean value	43.4	27.0	0.8	5.7	4.5	12.2	5.9	0.4
	Std. Dev.	14.4	5.5	0.3	1.7	1.4	4.5	1.7	0.1
	Max.	62.4	38.6	1.5	8.2	7.2	22.7	8.7	0.7
	Min.	14.6	19.5	0.5	3.0	2.8	6.8	3.2	0.3
RLA 450ºC total (3)	Mean value	40.7	27.5	1.0	6.0	5.2	12.9	6.2	0.5
	Std. Dev.	14.0	5.5	0.3	1.8	1.9	4.8	1.6	0.2
	Max.	62.5	38.6	1.6	9.0	10.7	24.2	9.3	1.2
	Min.	14.6	19.5	0.5	3.0	2.7	6.1	3.2	0.3
RLA 550ºC total (4)	Mean value	39.3	24.6	0.6	8.9	7.1	14.3	4.8	0.4
	Std. Dev.	9.7	2.0	0.1	2.7	2.8	4.1	1.5	0.1
	Max.	50.7	27.0	0.7	12.4	11.4	20.1	6.5	0.6
	Min.	26.6	22.1	0.4	5.0	3.9	9.6	3.1	0.3

(1) Calculated from analyses on 15 different areas.

(2) Calculated from analyses on 15 different areas.

(3) Combined results from (1) and (2).

(4) Calculated from analyses on 8 different areas.

Table 3. Mean values of chemical composition for rice leaf sheath ashes (RlsA) and rice stem ashes (RsA) (external, internal and both zones) obtained at 450°C. Values were calculated from EDS analysis on a 115 μm × 85 μm area. (Std. Dev = standard deviation; Max = maximum value recorded; Min = minimum value recorded)

Sample	Parameter	SiO_2	K_2O	Cl	CaO	MgO	P_2O_5	SO_3	Na_2O
RlsA 450ºC external (1)	Mean value	37.7	33.4	4.7	1.5	2.7	16.2	3.2	0.7
	Std. Dev.	17.8	5.8	2.0	1.6	1.6	7.2	1.1	0.4
	Max.	63.5	41.2	8.7	3.8	5.7	28.1	5.1	1.4
	Min.	9.8	24.5	1.3	0.00	0.5	7.4	1.3	0.2
RlsA 450ºC internal (2)	Mean value	23.3	40.6	6.9	1.0	3.4	18.1	4.9	1.3
	Std. Dev.	19.7	8.0	5.0	1.3	1.0	5.9	1.3	0.4
	Max.	59.8	49.4	16.5	3.0	4.6	25.8	7.0	2.0
	Min.	0.00	27.9	1.3	0.00	1.1	7.2	2.2	0.5
RlsA 450ºC total (3)	Mean value	32.0	36.3	5.6	1.3	3.0	17.2	3.9	0.9
	Std. Dev.	19.56	7.51	3.60	1.48	1.44	6.70	1.45	0.48
	Max.	63.5	49.4	16.5	3.8	5.7	28.1	7.0	2.0
	Min.	0.00	24.5	1.3	0.00	0.5	7.2	1.3	0.2
RsA 450ºC external (4)	Mean value	83.0	4.7	0.2	4.8	4.2	1.1	1.5	0.5
	Std. Dev.	7.2	2.1	0.2	2.4	2.8	0.8	0.8	0.2
	Max.	95.0	9.0	0.6	9.6	11.9	3.1	3.6	1.1
	Min.	67.3	2.1	0.00	0.8	1.3	0.00	0.6	0.2
RsA 450ºC internal (5)	Mean value	86.1	3.0	0.00	6.3	2.0	1.1	1.2	0.4
	Std. Dev.	2.4	0.5	0.00	1.1	0.7	0.3	0.4	0.1
	Max.	90.8	3.8	0.00	8.1	3.1	1.6	1.7	0.6
	Min.	83.3	2.3	0.00	4.1	1.2	0.8	0.6	0.2
RsA 450ºC total (6)	Mean value	84.3	4.0	0.1	5.4	3.4	1.1	1.4	0.5
	Std. Dev.	5.9	1.9	0.2	2.1	2.4	0.6	0.7	0.2
	Max.	95.0	9.0	0.6	9.6	11.9	3.1	3.6	1.1
	Min.	67.3	2.1	0.0	0.8	1.2	0.0	0.6	0.2

(1) Calculated from analyses on 15 different areas.

(2) Calculated from analyses on 15 different areas.

(3) Combined results from (1) and (2).

(4) Calculated from analyses on 15 different areas.

(5) Calculated from analyses on 15 different areas

(6) Combined results from (4) and (5).

Table 4. Compressive strengths (in MPa, standard deviation in parentheses) for mortars after 7 days and 28 days of curing.

Mortar	7 days	28 days
OPC control	54.9 (0.7)	62.7 (0.6)
10% RSA	54.1 (1.8)	67.1 (2.0)
25% RSA	45.8 (1.3)	58.9 (1.8)

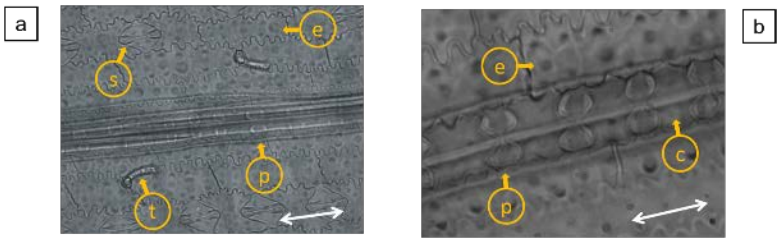

Fig. 1. Optical microscopy images of fresh rice leaf: a) adaxial (× 40) and b) abaxial surface (× 100). Key: p = phytolith; s = stoma; c = suberous cell; e = elongated epidermal cell; t = trichome; arrows indicate the longitudinal direction of the leaf.

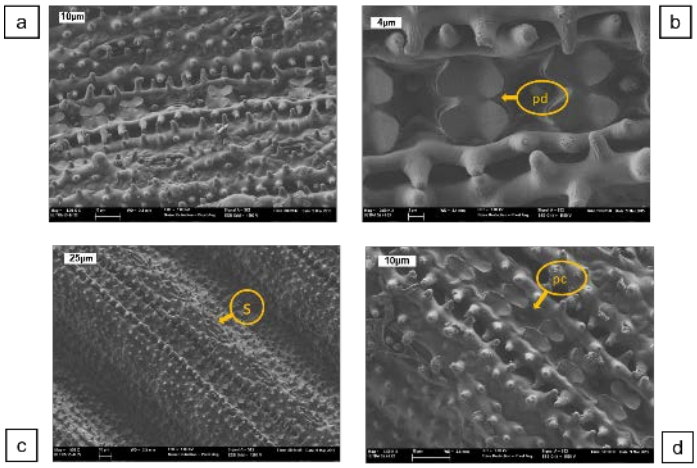

Fig. 2. FESEM micrographs of 105°C dried rice leaf: a) general view of adaxial surface; b) detailed view of dumbbell shape phytolith (pd); c) general view of abaxial surface; d) detailed view of cross shape phytolith (pc).

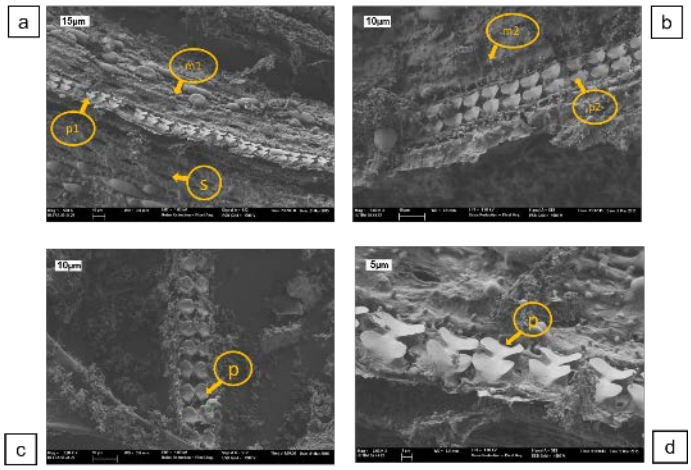

Fig. 3. FESEM micrographs for rice leaf calcined at 450°C. Key: p = phytolith; m = matrix; p1 and p2, phytolith spots; m1 and m2, matrix spots (see Table 2).

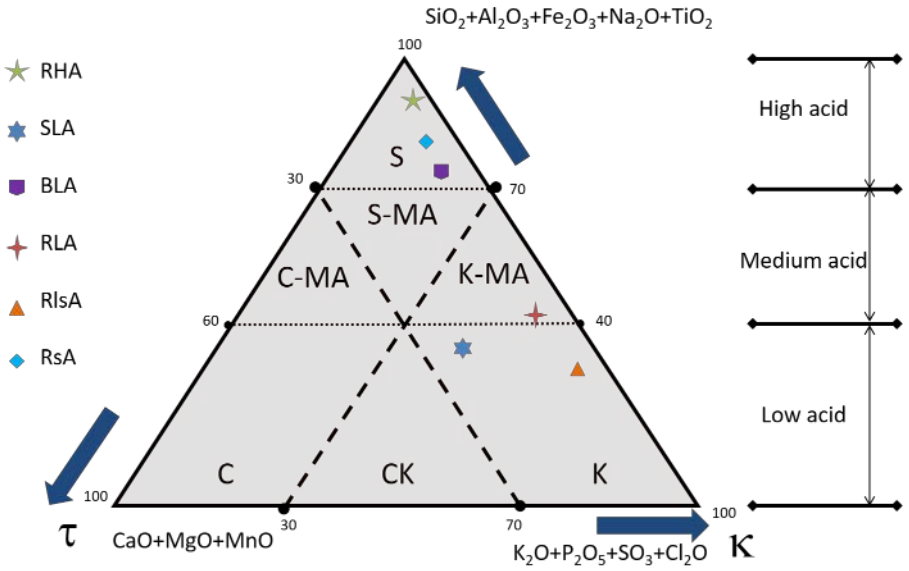

Fig. 4. Ternary diagram for the classification of biomass ashes (according to Vassilev et al., 2010). Location of some examples of reported agricultural waste ashes: rice husk ash (RHA), bamboo leaf ash (BLA), sugarcane leaf ash (SLA); location of ashes characterised in this research: rice leaf ash (RLA), rice leaf sheath ash (RlsA) and rice stem ash (RsA).

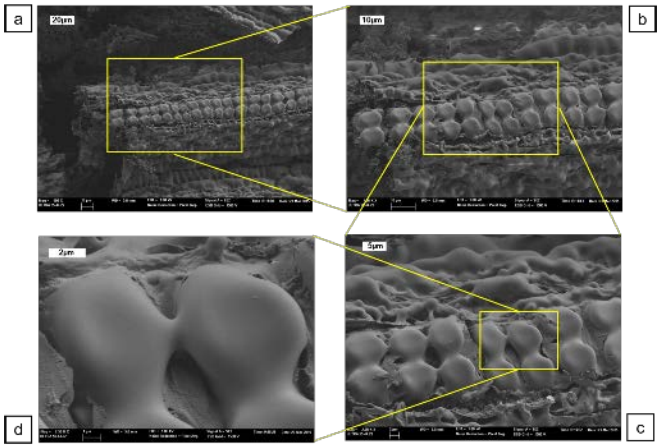

Fig. 5. FESEM micrographs of a RLA (adaxial surface) obtained at 550°C: a) general view of the spodogram; b) and c) enlarged zones; d) detailed view of sintered phytoliths.

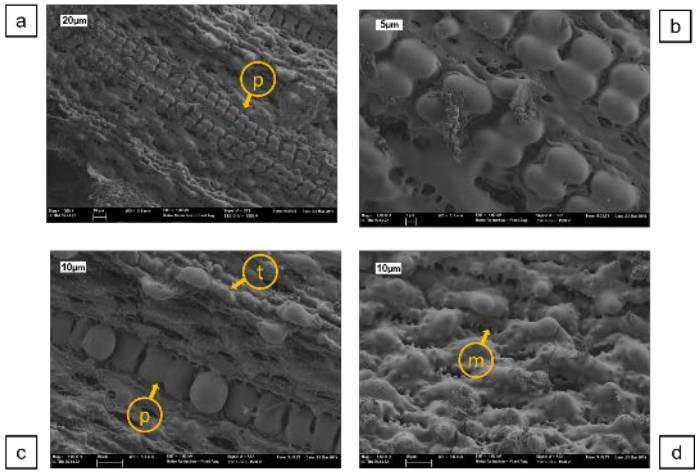

Fig. 6. FESEM micrographs of RLA (abaxial surface) obtained at 550°C: a) double chain of phytoliths; b) detail of the twin lines; c) highly spheroidal phytoliths; d) inorganic matrix.

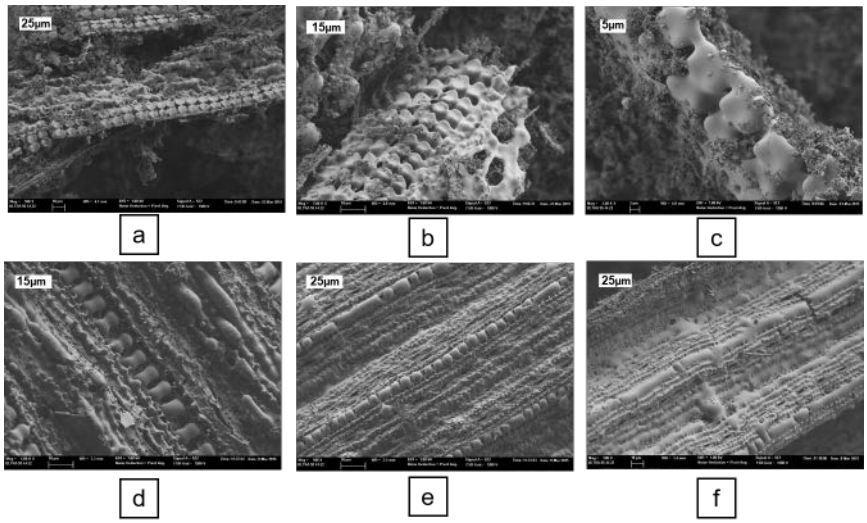

912

913 Fig. 7. FESEM micrographs for RLA obtained at 600°C (a, b, c: slightly sintered

914 phytoliths) and at 650°C (d, e, f: highly sintered phytoliths).

915

916

917

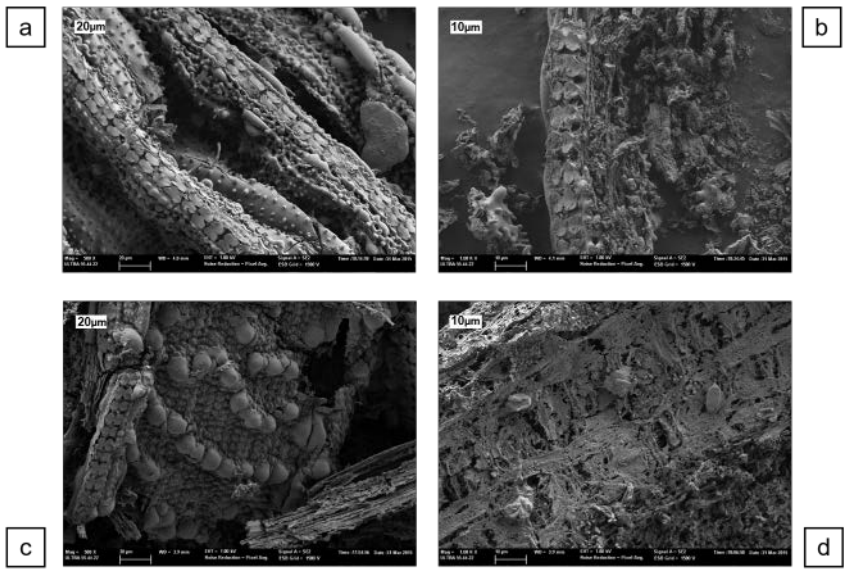

918

919 Fig. 8. FESEM micrographs of samples obtained at 450C: a) external part of the

920 stem; b) internal part of the stem; c) external part of the leaf sheath; d) internal

921 part of the leaf sheath.

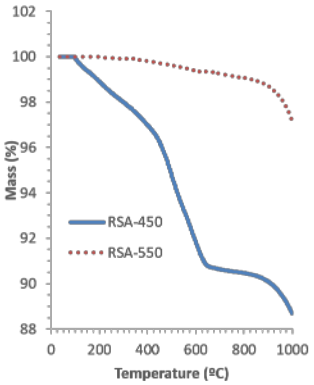

Fig. 9. Thermogravimetric curves for RSA-450 and RSA-550 (Dried air atmosphere, 20°C.min^{-1} heating rate).

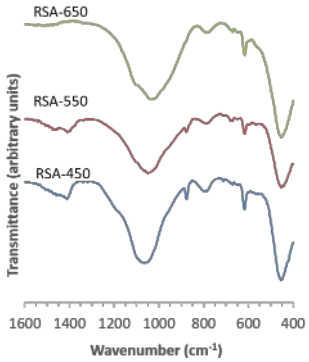

Fig. 10. FTIR spectra (400–1600 cm^{-1} range) for RSA-450, RSA-550 and RSA-650.

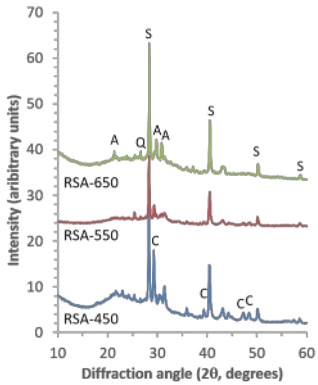

Fig. 11. XRD patterns for RSA-450, RSA-550 and RSA-650. Key: S = sylvite; C = calcite; Q = quartz; A = arcanite.

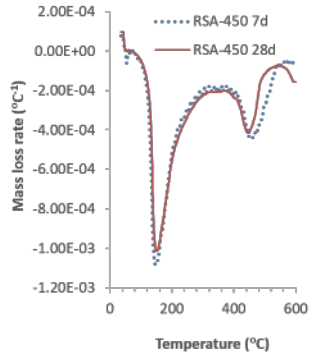

931

932 Fig. 12. DTG curves of RSA-450:CH (1:1) pastes cured for 7 and 28 days.

933

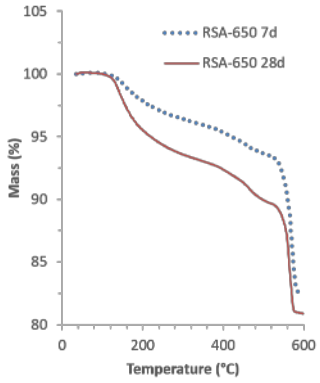

934

935 Fig. 13. TG curves of RSA-650:CH (3:7) pastes cured for 7 and 28 days.

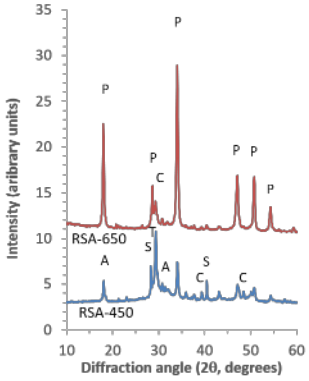

936

937 Fig. 14. XRD patterns for RSA-450:CH (1:1) paste and RSA-650:CH (3:7)

938 paste, both cured at room temperature for 28 days. Key: S = sylvite; C = calcite;

939 A = arcanite; P = portlandite; T = tobermorite.

940

941

942

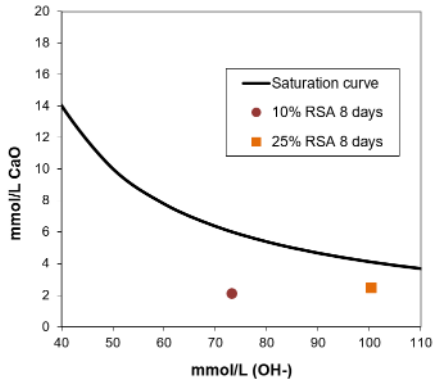

943

944 Fig.15. Frattini test results after 8 days curing at 40ºC for blended cements with

945 RSA (10% and 25% replacement percentages).

946

947